



Research article

Short spin waves excitation in spin Hall nano-oscillators

Mohammad Haidar

Department of Physics, American University of Beirut, P.O. Box 11-0236, Riad El-Solh, Beirut, 1107-2020, Lebanon



ARTICLE INFO

Keywords:

Spin Hall nano-oscillators

Spin Hall effect

Short spin wave propagation

ABSTRACT

This study investigates the excitation of short-wavelength spin waves (SWs) in nanowire-based spin-Hall nano-oscillators (SHNOs). Using micromagnetic simulations, we study the wavelength of propagating SWs as a function of nanowire width, ranging from 10 to 50 nm, excited in a 1.7 nm-thick CoFeB layer using a pure spin current generated by a 5 nm thin platinum layer via the spin Hall effect. Our results showed that SWs with shorter wavelengths are excited in narrow widths at higher magnetic fields and higher currents. In addition, the wavelength of the propagating waves scales linearly with the width of the nanowire. We attribute the emission of short wavelength due to the quantization of SWs in the nanowire. By reducing the nanowire width, SWs with ultrashort wavelengths are excited at high frequencies, with larger propagation speeds and longer attenuation lengths. Our results show that ultrashort SWs with wavelengths as short as 80 nm can be generated in metallic-based SHNOs, with a group velocity of $v_g = 1.6 \mu\text{m/ns}$ and attenuation length of $L_{att} = 0.6 \mu\text{m}$. These findings have significant implications for the scalability of magnonic devices, which could have potential applications in SW-based logic and neuromorphic computing.

1. Introduction

While the CMOS-based technology is approaching its fundamental constraints, high-performance electronic devices are experiencing extreme challenges in terms of power consumption and miniaturization [1]. Spin Wave (SW) excitation, i.e. the collective precession of the magnetization (M) in magnetic materials, offers a promising alternative as it allows for substantial low power consumption resulting from the absence of the ohmic losses [2,3]. In addition, SW-based technology allows for further scalability of devices, due to its shorter wavelengths (λ) which span a wide range from a macroscopic length down to nanometers [4]. Exchange-dominated SWs oscillate at high frequencies with short wavelengths below 100 nm and large group velocities. However, the excitation, manipulation, and propagation of SWs with short λ remain a crucial challenge [5–9]. Recently, the challenge of generating short SWs has been addressed using: wavelength conversion in magnonic waveguides [10], emission of SW from a pinned magnetic vortex cores [11] or domain wall [12], and coupling between periodic ferromagnetic structure and an adjacent ferrimagnetic film [13–17]. Indeed, propagating SWs can be effectively excited using spin-transfer torques mechanism [18–25], by utilizing spin-polarized current. In spin-Hall nano-oscillators (SHNOs) devices, SWs could be excited with $\lambda = 250 \text{ nm}$ [26–29] however, a systematic study to examine ultrashort SWs excitation in these devices is still lacking.

In this paper, we study the excitation of propagating SWs with short wavelengths in nanowire-based spin-Hall oscillators while varying the

width of the nanowire, $w = 10\text{--}50 \text{ nm}$. We employ micromagnetic simulations to determine λ of propagating SWs as a function of w in 1.7 nm thin CoFeB layer. Our results showed that SWs with shorter λ are excited in narrow widths at higher magnetic fields and higher currents. In addition, we find a linear relation between λ and w . We attribute the emission of short wavelength due to the quantization of SWs in the nanowire. While reducing w , SWs with ultrashort wavelengths are excited at high frequencies, with larger propagation speeds and longer attenuation lengths. Our results show that ultrashort SWs with wavelengths as short as 80 nm can be generated in metallic-based SHNOs, with a group velocity of $v_g = 1.6 \mu\text{m/ns}$, and an attenuation length of $L_{att} = 0.6 \mu\text{m}$. This is a promising result where the integration of SHNOs in magnonics may lead to further scalability of electronic devices.

2. Methods

As a basis for the micromagnetic simulations, we simulate a stack of, 1.7 nm CoFeB and 5 nm Pt layers containing a rectangular-shaped nanowire of length $l = 200 \text{ nm}$ and w which is varied between 10, 20, and 50 nm as shown in Fig. 1(a). An in-plane current is applied along the y -direction where a high current density is centered in the nanowire regime and decays rapidly in the electrodes. The electrical current density and the corresponding Oersted field in the devices were simulated using COMSOL software under a reference electrical current of 2 mA. A plot of the maximum electrical current density versus w is

E-mail address: mh280@aub.edu.lb.<https://doi.org/10.1016/j.jmmm.2023.171336>

Received 12 July 2023; Received in revised form 28 September 2023; Accepted 30 September 2023

Available online 5 October 2023

0304-8853/© 2023 Elsevier B.V. All rights reserved.

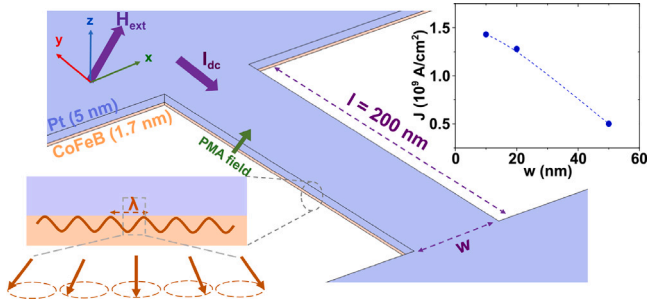


Fig. 1. (a) Schematic layout of the nanowire-based spin-Hall oscillator device made of CoFeB (1.7 nm)/Pt (5 nm) bilayer with a nanowire of width (w) and length $l = 200$ nm. This shows the direction of the applied magnetic field and the dc current. (inset) The maximum current density as a function of w calculated at $I = 2$ mA using COMSOL software.

shown in Fig. 1(b) where the current density is inversely proportional to w . The micromagnetic simulations are performed using mumax³ solver with the input from the COMSOL simulation. In the simulations, we assume a rectangular mesh which has dimensions of $2000 \times 2000 \times 1.7$ nm³ with a cell size of $3.9 \times 3.9 \times 1.7$ nm³. We translate the electrical current density (J_e) to the spin current density (J_s), using the relation $J_s = \theta_{SH} J_e$ where θ_{SH} is the spin Hall angle of Pt and is equal to 0.1. In the simulation we assume that the injected spin current produces mainly a damping-like torque of the Slonczewski form, more details can be found in Dvornik et al. [30]. For micromagnetic simulations, the CoFeB/Pt bilayers were assumed to have a saturation magnetization $\mu_0 M_s = 0.9$ T, a Gilbert damping $\alpha = 0.02$, a gyromagnetic ratio $\gamma/2\pi = 30$ GHz/T, and an exchange stiffness of $A = 15$ pJ/m, consistent with experimental studies [31]. The magnetization dynamics are simulated by integrating the Landau–Lifschitz–Gilbert–Slonczewski (LLG-S) equation over 200 ns. The frequencies and spatial profiles of excited modes of the system are extracted by performing the Fast Fourier Transform (FFT) of the time domain data that represents the evolution of the magnetization.

3. Results and discussion

First, we study the spin-torque-driven auto-oscillations in devices while considering a perpendicular magnetic anisotropy (PMA) $K_u = 0.075$ MJ/m³ [28,31]. An out-of-plane magnetic field $\mu_0 H = 0.7$ T is applied at 75° to the nanowire. When an in-plane dc current (I) is injected into the nanowire high-intensity auto-oscillations are detected while scanning I up to 1.5 mA in each device. In Fig. 2(a–c), the power spectral density of SWs is recorded in the three devices, where the dashed line represents the Ferromagnetic resonance (FMR) mode of the full device. Current-induced SW auto-oscillations are observed when a pure spin current generated by the spin Hall effect counteracts the natural damping of the devices and allows for the emission of high-intensity oscillations above a threshold current. The frequency of the auto-oscillations lies above the frequency of the linear mode and is tunable with the applied current. Although the threshold current seems to be similar in Fig. 2, the current density is different for the three devices that drive propagating waves with different onset frequencies. Note that the frequency of the auto-oscillations is higher in the 10-nm device as compared to other devices. This mode corresponds to the excitation of propagating SW in nanowire devices [29].

Then, we determine λ of the propagating SW while varying w , $\mu_0 H$, and I . We obtain λ by calculating the magnetization profile of the oscillations at $\mu_0 H = 0.7$ T and $I = 1$ mA. Fig. 3 shows the spatial mode profile of the z -component of magnetization (m_z) for three different devices, (a) 10 nm, (b) 20 nm, and (c) 50 nm, where the oscillations begin in the center of the nanowire and propagate into the leads. Current devices can generate cylindrical waves emerging from the nanowire into the electrodes with a controlled wavelength which is interesting

to use SHNOs devices as microwave emitters in magnonic. The shapes of the modes differ in the nanowire since the oscillations have different wavelengths as we will discuss below. To determine λ , we extract the magnitude of m_z along the y -direction, at $x = 0$ where m_z exhibits a high amplitude of oscillation at the center of the nanowire that decays exponentially away from the center and propagate into the leads of the device as shown in Fig. 3(d). We measure shorter SW excitations with shorter λ in the 10 nm device. This observation suggests that altering the width of the nanowire results in the excitation of propagating waves with different wave vectors due to the confinement of SWs. Fig. 3(e) shows the magnitude of m_z extracted along the width of the nanowire, at $y = 0.0$ μ m. All three devices exhibit a cosine-like profile, similar to previous investigations of confined waveguides [34]. Notably, the amplitude of m_z at the edges displays a 100% change for the 50 nm devices i.e. it is almost null at one of edge, while a symmetric profile is observed for the 20 nm devices, and a weaker change of 10% is recorded for the 10 nm devices. This behavior could arise from strong confinement of Sws across the nanowire while reducing the width, influenced by different pinning conditions for the magnetization at the edges in each device, and consequently modifying the SW dispersion relation [35]. We report a linear variation between λ and w as shown in Fig. 4(a). Reducing the nanowire width results in stronger confinement leading to the emission of propagating waves with shorter wavelengths. This is consistent with the Slonczewski relation derived for the nano-contact geometry where the wavevector (k) of the emitted waves is inversely related to the radius of the nanocontact r_{NC} with $k = 1.2/r_{NC}$ [36].

While increasing the magnetic field from 0.7 T (closed circles) to 0.9 T (open circles), a further reduction in λ is observed. This is due to a change in the magnetization orientations at the edges, i.e. the boundary conditions, which affects λ of the propagating waves. Consequently, the propagating waves oscillate at higher frequencies while reducing w and increasing the magnetic fields, as shown in Fig. 4(b).¹ To investigate the effect of the current on λ , we calculate λ at a constant field of 0.7 T and constant currents of 0.6, 0.8, and 1.0 mA. The results are presented in the inset of Fig. 4(a). It is observed that λ can be adjusted by changing the current, and higher currents result in the excitation of shorter λ propagating SWs in each device. This can be attributed to the increased strength of the spin-torque as the dc current rises, allowing for the excitation of propagation with short λ . Additionally, the Oersted field generated around the vicinity of the nanowire increases with the applied current, contributing to the change in the net field and the frequency of the excited SWs [37] and hence results in a change in λ . In our study, we detect an ultra-short λ of 80 nm for the 10 nm nanowire device, and by further reducing the width to sub-nanometer dimensions, a minimum λ of 60 nm could be achieved in such devices. Table 1 summarizes the results presented in this study and other studies where short wavelengths are generated by various mechanisms. Note that the characteristics of propagating waves in present SHNOs devices are well compared with insulator-based devices. Finally, we extract the properties of the propagating SW in SHNOs, which include the wave vector (k), group velocity (v_g), and attenuation length (L_{att}). The results presented in Fig. 5 are obtained using the following parameters $\mu_0 H = 0.7$ T, $K_u = 0.075$ MJ/m³, and $I = 1$ mA. The wave vector k of SWs is determined analytically from the dispersion relation (blue square) of propagating spin waves considering thin film approximation [38] while taking into account the exchange interaction and perpendicular magnetic anisotropy,

$$\omega = \left(\frac{\mu_0 \gamma}{2\pi} \right) \sqrt{(H_M + Dk^2) (H_M + Dk^2 + M_{eff} \cos(\theta_M))} \quad (1)$$

where M_{eff} is the effective magnetization $M_{eff} = M_s - H_k$, with $H_k = \frac{2K_u}{M_s}$ is the PMA field. The effective internal magnetic field

¹ When K_u exceeds the threshold for generating propagating SWs, both the frequency and wavelength of the emitted waves increases.

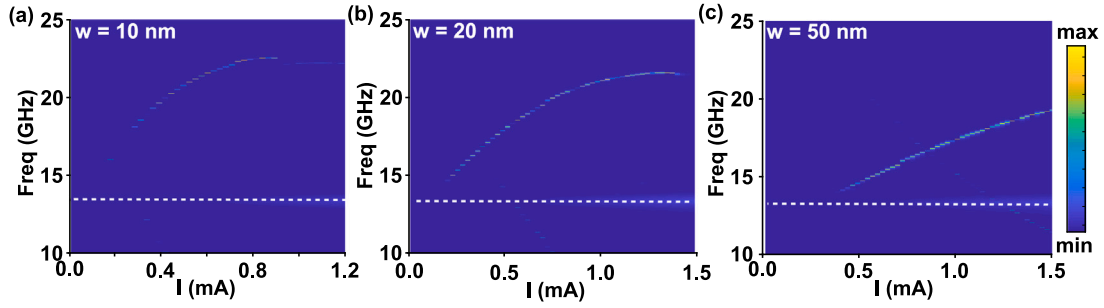


Fig. 2. Color plot of the power spectra of spin-wave modes in CoFeB/Pt nanowires with different widths (a) 10 nm, (b) 20 nm, and (c) 50 nm, as a function of dc current. The dashed line represents the FMR mode of the full device. The micromagnetic simulations were carried out under an applied magnetic field of 0.7 T at an out-of-plane angle of 75° with a perpendicular magnetic anisotropy $K_u = 0.075 \text{ MJ/m}^3$.

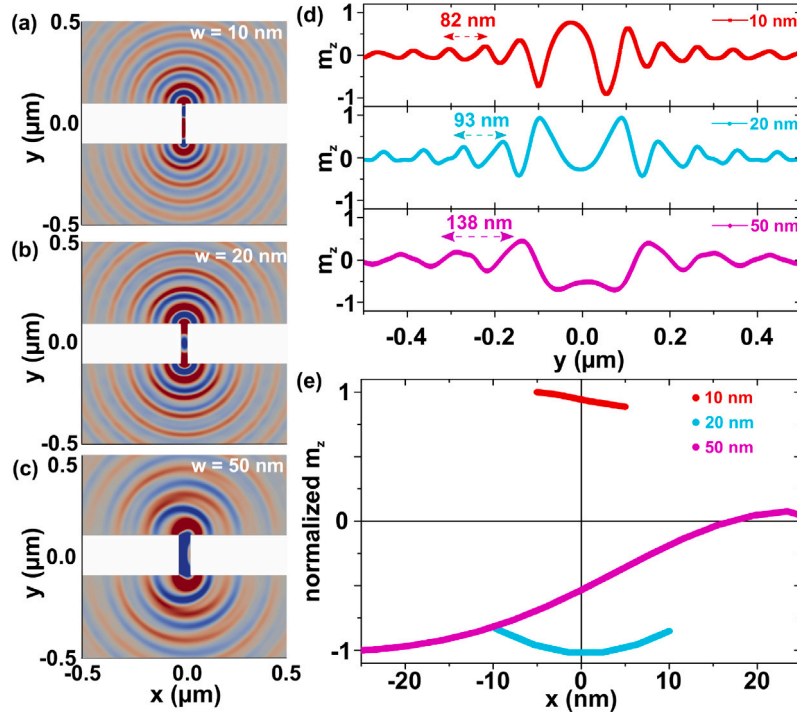


Fig. 3. The calculated spatial mode profile of the z-component of the magnetization (m_z) for nanowire devices of (a) 10 nm, (b) 20 nm, and (c) 50 nm widths. Variation of m_z as a function of at (d) $x = 0.0 \mu\text{m}$ and (e) $y = 0.0 \mu\text{m}$ for the three devices. The mode profiles are calculated for 0.7 T at $I = 1 \text{ mA}$ and $K_u = 0.075 \text{ MJ/m}^3$.

Table 1

Comparison of the propagating spin wave characteristics excited in different devices.

| Layer | Devices | Frequency (GHz) | λ (μm) | v_g ($\mu\text{m/ns}$) | Ref |
|------------------------------------------------|--------------------------|-----------------|-----------------------------|----------------------------|------------|
| YIG(20 nm)/Ti(1 nm)/CoFe(50 nm) | Nanowire/thin films | 26.5 | 0.05 | 2.6 | [15] |
| YIG(20 nm)/Ni80Fe20(15 nm) | Nanowire/nanodisks | 17 | 0.088 | 1.2 | [14] |
| Ni81Fe19 discs | Vortex core | 10 | 0.08 | 0.55 | [32] |
| YIG (44 nm) | Conduit | 3.84 | 0.6 | 0.1 | [16] |
| Co81Fe19(20 nm)/Cu(6 nm)/Ni80Fe20(4.5 nm) | Spin-torque | 15.3 | 2.1 | 3.3 | [26] |
| CoFeB/MgO/CoFe | Magnetic tunnel junction | 24.7 | 0.07 | 1.65 | [33] |
| Bi-YIG (20 nm)/Pt(6 nm) | Spin Hall effect | 5.6 | 0.3 | 0.13 | [27] |
| β -W(5 nm)/Co20Fe60B20(1.4 nm)/MgO(2 nm) | Spin Hall effect | 10 | 0.285 | 1.3 | [28] |
| CoFeB(1.7 nm)/Pt (5 nm) | Spin Hall effect | 22.5 | 0.08 | 1.6 | This study |

and angle are calculated using magnetostatic approximation, as $H_M = 0.258 \text{ T}$ and $\theta_M = 0.79 \text{ rad}$, respectively. We report an increase in k as w decrease, where k varies between 42 and $74 \text{ rad}/\mu\text{m}^{-1}$ for 50 and 10 nm respectively, as shown in Fig. 5 (main panel). The group velocity v_g is determined from the dispersion relation as $v_g = \frac{d\omega}{dk} \approx \frac{4\gamma Ak}{M_{eff}}$. SWs in these devices propagate at high velocities, ranging from 0.95 to $1.6 \mu\text{m/ns}$ for 50 and 10 nm respectively, as shown in the inset of Fig. 5 (blue squares). Notably, large speeds are achieved for waves

with higher k , which correspond to the 10 nm width nanowire. The effectiveness of SW radiation is estimated by calculating the attenuation length L_{att} from the group velocity v_g , using the equation $L_{att} = \frac{v_g}{\alpha\omega}$. We calculate an increase in L_{att} from 0.46 to $0.56 \mu\text{m}$ as k increases from 42 and $74 \text{ rad}/\mu\text{m}^{-1}$, as shown in the inset of Fig. 5 (red circles). In this study, we notice that the amplitude of SWs decays faster for SWs with lower k where we report an increase in the L_{att} by a factor of 1.2 while increasing k .

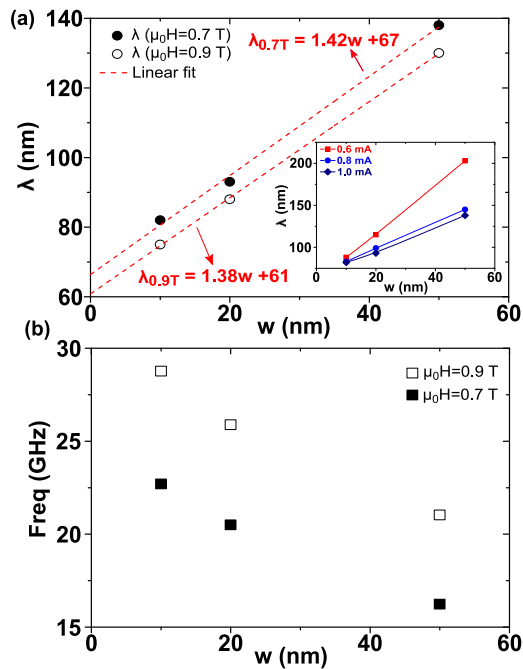


Fig. 4. (a) Variation of the spin-wave wavelength λ versus w of the device at 0.7 T (closed dots) and 0.9 T (open dots) with $I = 1$ mA and $K_u = 0.075$ MJ/m³. Red lines are linear fits. (Inset) The change of λ versus w at different values of I with a magnetic field of $\mu_0 H = 0.7$ T. (b) Variation of frequency versus w measured at 0.7 T (closed dots) and 0.9 T (open squares) with $I = 1$ mA and $K_u = 0.075$ MJ/m³.

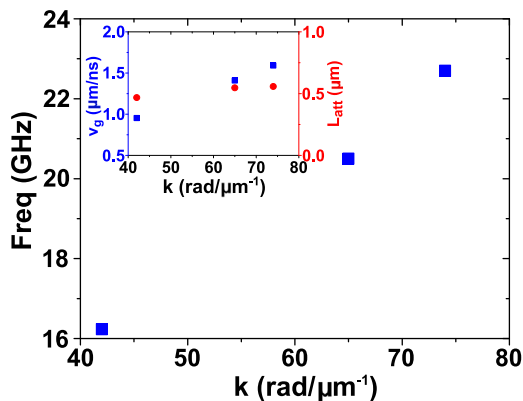


Fig. 5. (a) Variation of frequency versus k (blue symbols). (inset) Variation of v_g (blue squares) and L_{att} (red circles) as a function of k . The characteristics of the propagating waves are calculated for 0.7 T (closed dots) at $I = 1$ mA and $K_u = 0.075$ MJ/m³.

Overall, reducing the width of the nanowire results in propagating waves with (i) shorter λ , higher k or equivalently higher frequencies, (ii) larger v_g , and (iii) slightly longer propagation distances. This latter is critical for applications where longer L_{att} is desired for implementing metallic magnetic films in SW-based logic and neuromorphic computing technologies. Since L_{att} is inversely proportional to the damping coefficient a longer attenuation length could be achieved while fabricating nanowire devices with low damping materials [22, 39].

4. Conclusion

In summary, this paper presents the successful generation of short-wavelength propagating SWs in nanowire-based spin-Hall oscillators with a width as small as 10 nm. The results demonstrate that the wavelength of SWs can be adjusted by changing the nanowire width,

the applied magnetic field, and the current. We attribute the emission of short wavelength to the quantization of SW. An ultrashort SW excitation with a wavelength of 80 nm is achieved. Moreover, the study reveals that decreasing the nanowire width leads to the excitation of shorter wavelengths at higher frequencies, with larger propagation speeds and over longer distances. Pushing the SW wavelength to sub 100 s of nanometers allow the operation of magnonic devices at high frequencies ($f \propto k^2$) and at a faster data transmission ($v_g \propto k$). These findings provide valuable insights for designing SW devices with ultrashort wavelengths that could be beneficial for various SW-based logic and neuromorphic computing applications in the future.

CRediT authorship contribution statement

Mohammad Haidar: Data curation, Investigation, Conceptualization, Methodology, Validation, Writing – review & editing.

Declaration of competing interest

The authors declare that they have no known competing financial interests or personal relationships that could have appeared to influence the work reported in this paper.

Data availability

Data will be made available on request.

Acknowledgments

This work was supported by the American University of Beirut Research Board (URB), and the Mamdouha El-Sayed Bobst Deanship Fund.

References

- [1] Beyond CMOS, IEEE international roadmap for devices and systems, 2018, <https://irds.ieee.org/home/what-is-beyond-cmos>.
- [2] A.V. Chumak, V. Vasyuchka, A. Serga, B. Hillebrands, *Nat. Phys.* 11 (2015) 453.
- [3] B. Dieny, L.L. Prejbeanu, K. Garello, P. Gambardella, P. Freitas, R. Lehnndorff, W. Raberg, U. Ebels, S.O. Demokritov, J. Åkerman, A. Deac, P. Pirro, C. Adelman, A. Anane, A.V. Chumak, A. Hirohata, S. Mangin, S.O. Valenzuela, M.C. Onbaşlı, M. d'Aquino, G. Prenat, G. Finocchio, L. Lopez-Diaz, R. Chantrell, O. Chubykalo-Fesenko, P. Bortolotti, *Nat. Electron.* 3 (2020) 446.
- [4] A. Gurevich, G. Melkov, *Magnetization Oscillations and Waves*, CRC, New York, 2018.
- [5] V.V. Kruglyak, S.O. Demokritov, D. Grundler, *J. Phys. D: Appl. Phys.* 43 (2010) 264001.
- [6] V. Vlamincik, M. Bailleul, *Phys. Rev. B* 81 (2010) 014425.
- [7] M. Haidar, M. Bailleul, M. Kostylev, Y. Lao, *Phys. Rev. B* 89 (2014) 094426.
- [8] S. Rezende, F. de Aguiar, *Proc. IEEE* 78 (1990) 893.
- [9] T. Brä, P. Pirro, B. Obry, A.A. Serga, B. Hillebrands, *Appl. Phys. Lett.* 99 (2011) 162501, <http://dx.doi.org/10.1063/1.3651506>.
- [10] V.E. Demidov, M.P. Kostylev, K. Rott, J. Mü, G. Reiss, S.O. Demokritov, *Appl. Phys. Lett.* 99 (2011) 082507, <http://dx.doi.org/10.1063/1.3631756>.
- [11] S. Wintz, V. Tiberkevich, M. Weigand, J. Raabe, J. Lindner, A. Erbe, A. Slavin, J. Fassbender, *Nature Nanotechnol.* 11 (2016) 948.
- [12] B. Van de Wiele, S.J. Hä, P. Baláz, F. Montoncello, S. van Dijken, *Sci. Rep.* 6 (2016) 21330.
- [13] C.W. Sandweg, Y. Kajiwar, A.V. Chumak, A.A. Serga, V.I. Vasyuchka, M.B. Jungfleisch, E. Saitoh, B. Hillebrands, *Phys. Rev. Lett.* 106 (2011) 216601.
- [14] H. Yu, O. d'Allivy Kelly, V. Cros, R. Bernard, P. Bortolotti, A. Anane, F. Brandl, F. Heimbach, D. Grundler, *Nature Commun.* 7 (2016) 11255.
- [15] C. Liu, J. Chen, T. Liu, F. Heimbach, H. Yu, Y. Xiao, J. Hu, M. Liu, H. Chang, T. Stueckler, Y. Tu, S. Zhang, Y. Zhang, P. Gao, Z. Liao, D. Yu, K. Xia, N. Lei, W. Zhao, M. Wu, *Nature Commun.* 9 (2018) 738.
- [16] B. Heinz, T. Brä, M. Schneider, Q. Wang, B. Lä, A.M. Friedel, D. Breitbach, S. Steinert, T. Meyer, M. Kewenig, C. Dubs, P. Pirro, A.V. Chumak, *Nano Lett.* 20 (2020) 4220.
- [17] T. Bö, M. Ruhwedel, K.O. Levchenko, Q. Wang, H.L. Chumak, M.A. Popov, I.V. Zavislyak, C. Dubs, O. Surzhenko, B. Hillebrands, A.V. Chumak, P. Pirro, *Appl. Phys. Lett.* 120 (2022) 102401, <http://dx.doi.org/10.1063/5.0082724>.
- [18] J. Slonczewski, *J. Magn. Magn. Mater.* 159 (1996) L1.
- [19] L. Berger, *Phys. Rev. B* 54 (1996) 9353.

- [20] W.H. Rippard, M.R. Pufall, S.E. Russek, *Phys. Rev. B* 74 (2006) 224409.
- [21] V.E. Demidov, S. Urazhdin, H. Ulrichs, V. Tiberkevich, A. Slavin, D. Baither, G. Schmitz, S.O. Demokritov, *Nature Mater.* 3459 (2012) 1028.
- [22] M. Haidar, A. Awad, M. Dvornik, R. Khymyn, A. Houshang, J. Åkerman, *Nature Commun.* 10 (2019) 2362.
- [23] M. Ranjbar, P. Dürrenfeld, M. Haidar, E. Iacocca, M. Balinskiy, T.Q. Le, M. Fazlali, A. Houshang, A. Awad, R. Dumas, J. Åkerman, *IEEE Magn. Lett.* 5 (2014) 3000504.
- [24] V.E. Demidov, S. Urazhdin, A. Zholud, A.V. Sadovnikov, S.O. Demokritov, *Appl. Phys. Lett.* 105 (2014) 172410.
- [25] M. Haidar, H. Mazraati, P. Dü, H. Fulara, R. M., J. Åkerman, *Appl. Phys. Lett.* 118 (2021) 012406.
- [26] M. Madami, S. Bonetti, G. Consolo, S. Tacchi, G. Carlotti, G. Gubbiotti, F.B. Mancoff, M.A. Yar, J. Åkerman, *Nat. Nanotechnol.* 6 (2011) 635.
- [27] M. Evelt, L. Soumah, A. Rinkevich, S. Demokritov, A. Anane, V. Cros, J. Ben Youssef, G. de Loubens, O. Klein, P. Bortolotti, V. Demidov, *Phys. Rev. Appl.* 10 (2018) 041002.
- [28] H. Fulara, M. Zahedinejad, R. Khymyn, A.A. Awad, S. Muralidhar, M. Dvornik, J. Åkerman, *Sci. Adv.* 5 (2019) <http://dx.doi.org/10.1126/sciadv.aax8467>.
- [29] M. Succar, M. Haidar, *J. Appl. Phys.* 133 (2023) 093901.
- [30] M. Dvornik, A.A. Awad, J. Åkerman, *Phys. Rev. Appl.* 9 (2018) 014017.
- [31] M. Zahedinejad, H. Mazraati, H. Fulara, J. Yue, S. Jiang, A.A. Awad, J. Åkerman, *Appl. Phys. Lett.* 112 (2018) 132404.
- [32] G. Dieterle, J. Förster, H. Stoll, A.S. Semisalova, S. Finizio, A. Gangwar, M. Weigand, M. Noske, M. Fähnle, I. Bykova, J. Gräfe, D.A. Bozhko, H.Y. Musiienko-Shmarova, V. Tiberkevich, A.N. Slavin, C.H. Back, J. Raabe, G. Schütz, S. Wintz, *Phys. Rev. Lett.* 122 (2019) 117202.
- [33] A. Houshang, R. Khymyn, H. Fulara, A. Gangwar, M. Haidar, S.R. Etesami, R. Ferreira, P.P. Freitas, M. Dvornik, R.K. Dumas, J. Åkerman, *Nature Commun.* 9 (2018) 4374.
- [34] Q. Wang, B. Heinz, R. Verba, M. Kewenig, P. Pirro, M. Schneider, T. Meyer, B. Lägel, C. Dubs, T. Brächer, A.V. Chumak, *Phys. Rev. Lett.* 122 (2019) 247202.
- [35] K.Y. Guslienko, A.N. Slavin, *Phys. Rev. B* 72 (2005) 014463.
- [36] J. Slonczewski, *J. Magn. Magn. Mater.* 195 (1999) L261.
- [37] R.K. Dumas, E. Iacocca, S. Bonetti, S.R. Sani, S.M. Mohseni, A. Eklund, J. Persson, O. Heinonen, J. Åkerman, *Phys. Rev. Lett.* 110 (2013) 257202.
- [38] A. Slavin, V. Tiberkevich, *IEEE Trans. Magn.* 45 (2009) 1875.
- [39] D. Schoen, M.A.W. Thonig, M.L. Schneider, T.J. Silva, H.T. Nembach, O. Eriksson, O. Karis, J.M. Shaw, *Nat. Phys.* 12 (2016) 839.